

Memristors with diffusive dynamics as synaptic emulators for neuromorphic computing

Zhongrui Wang^{1†}, Saumil Joshi^{1†}, Sergey E. Savel'ev², Hao Jiang¹, Rivu Midya¹, Peng Lin¹, Miao Hu³, Ning Ge³, John Paul Strachan³, Zhiyong Li³, Qing Wu⁴, Mark Barnell⁴, Geng-Lin Li⁵, Huolin L. Xin⁶, R. Stanley Williams³, Qiangfei Xia¹, and J. Joshua Yang^{1*}

¹Department of Electrical and Computer Engineering, University of Massachusetts, Amherst, MA 01003, USA

²Department of Physics, Loughborough University, Loughborough LE11 3TU, UK

³Hewlett Packard Labs, Palo Alto, California 94304, USA

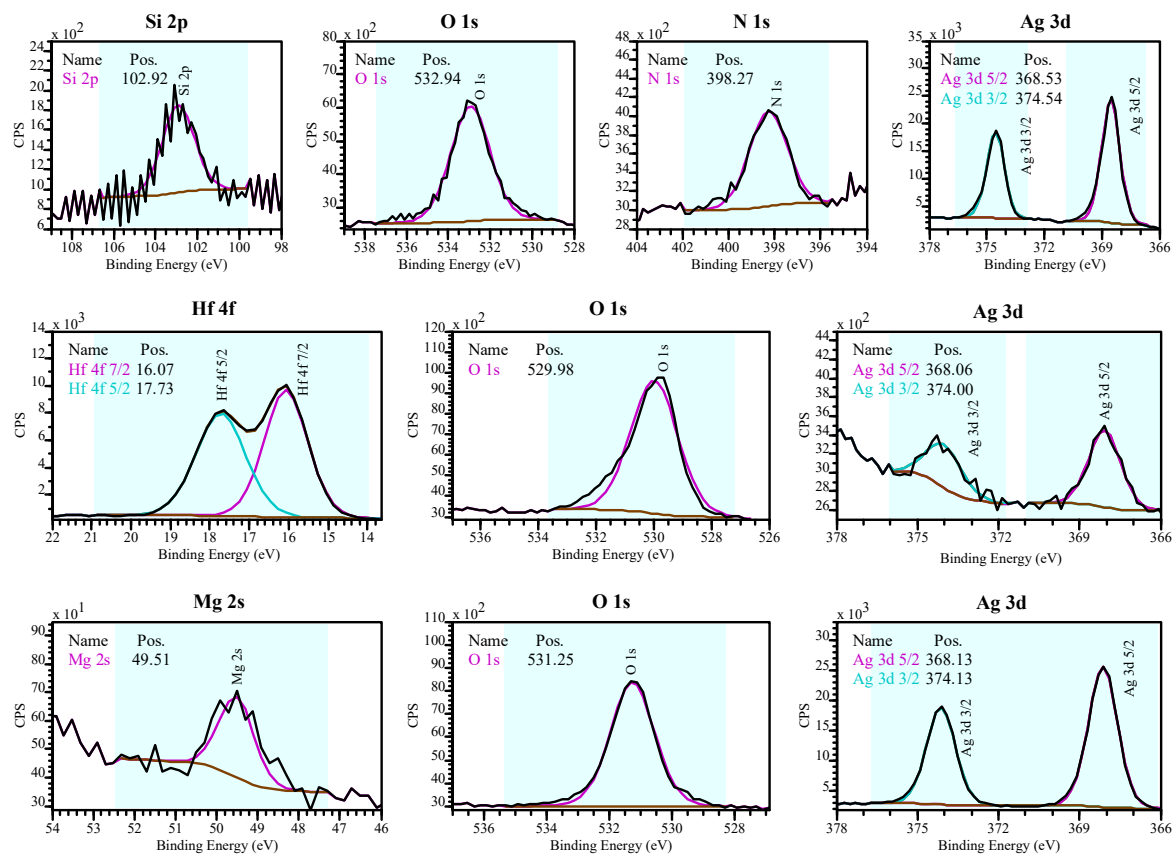
⁴Air Force Research Lab, Information Directorate, Rome, New York 13441, USA

⁵Biology Department, University of Massachusetts, Amherst, MA 01003, USA

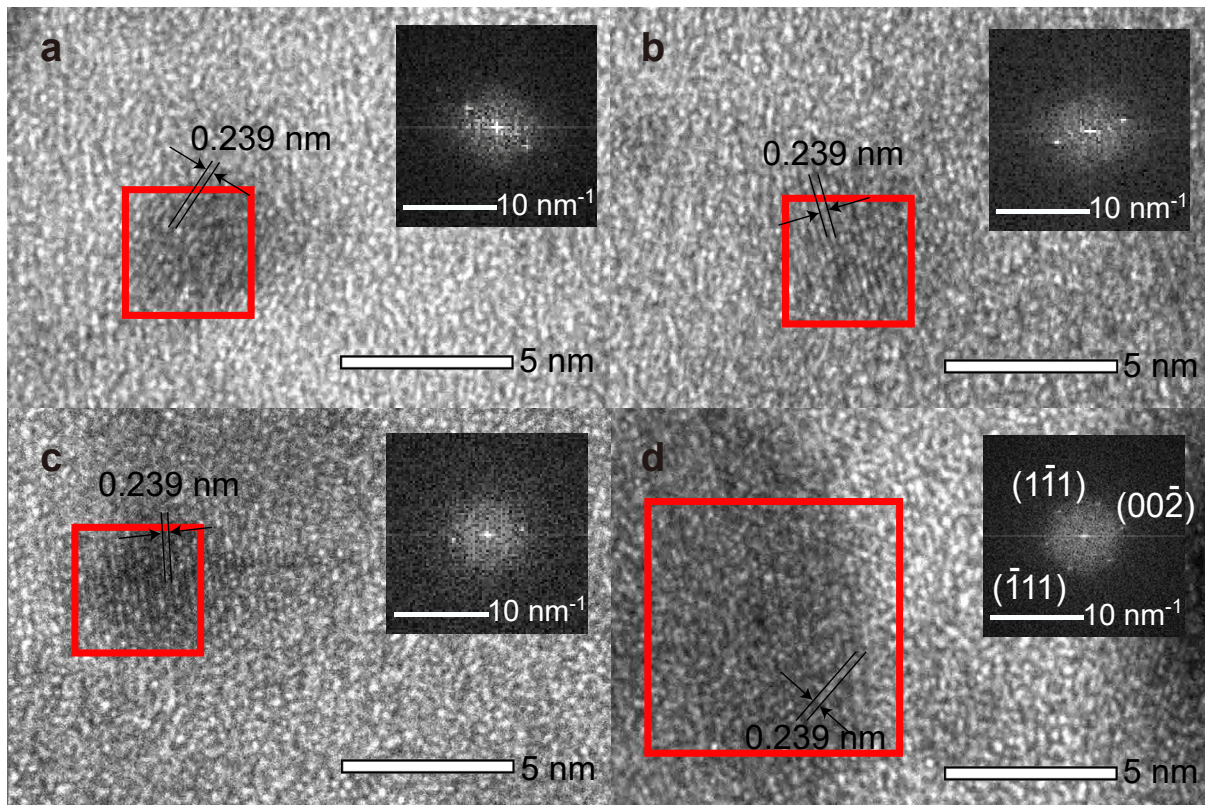
⁶Center for Functional Nanomaterials, Brookhaven National Laboratory, Upton, New York 11973, USA

[†]These authors contributed equally to this work.

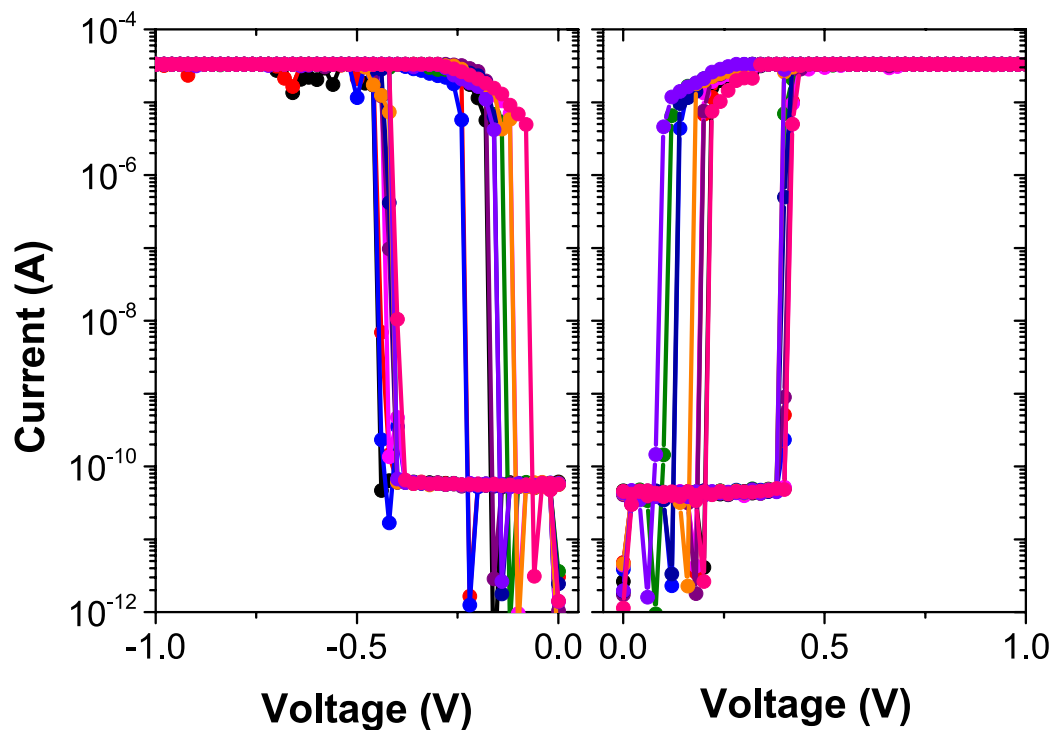
*e-mail: jjyang@umass.edu



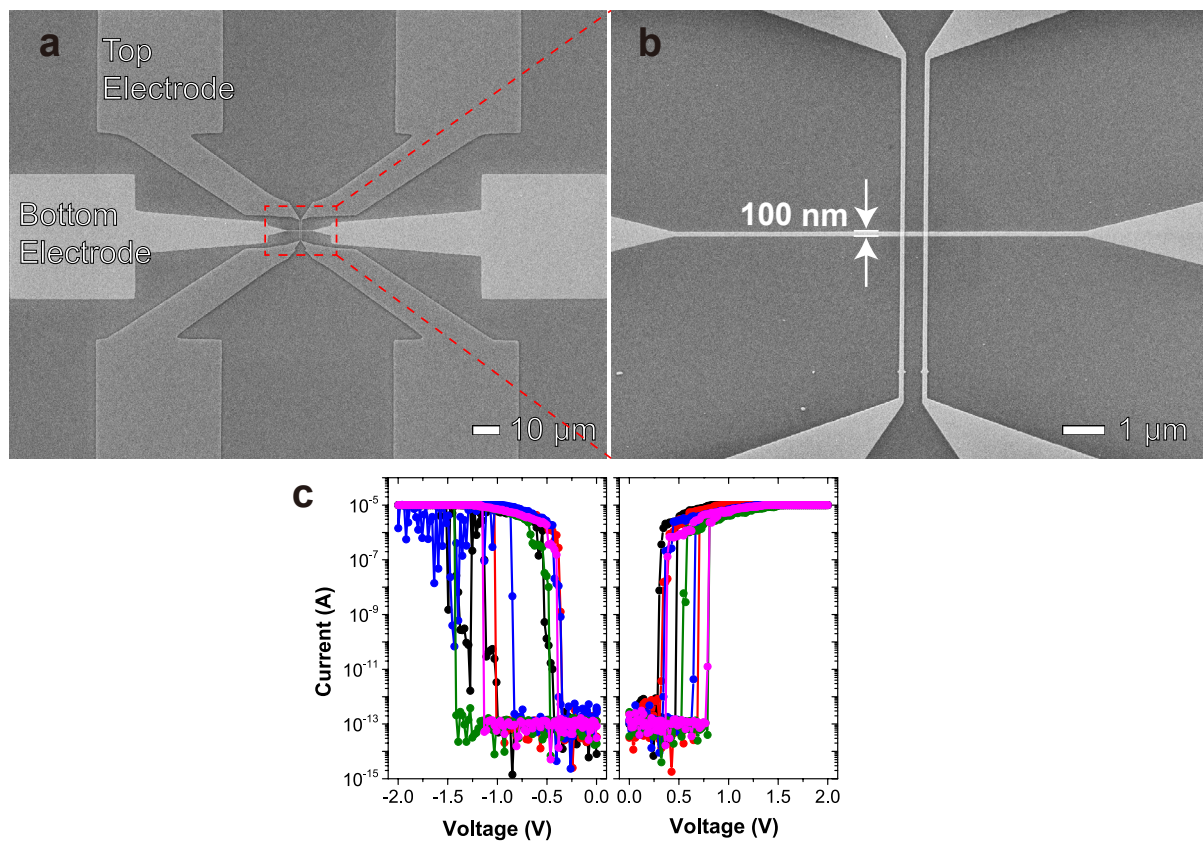
Supplementary Figure S1 X-ray Photoelectron Spectroscopy (XPS) of (a-d) $\text{SiO}_x\text{Ny:Ag}$ (e-g) $\text{HfO}_x\text{:Ag}$, and (h-j) $\text{MgO}_x\text{:Ag}$ films. All spectrums are calibrated by align C 1s to 284.6 eV. The binding energy of Ag in all three systems indicate a metallic nature of majority Ag particles.



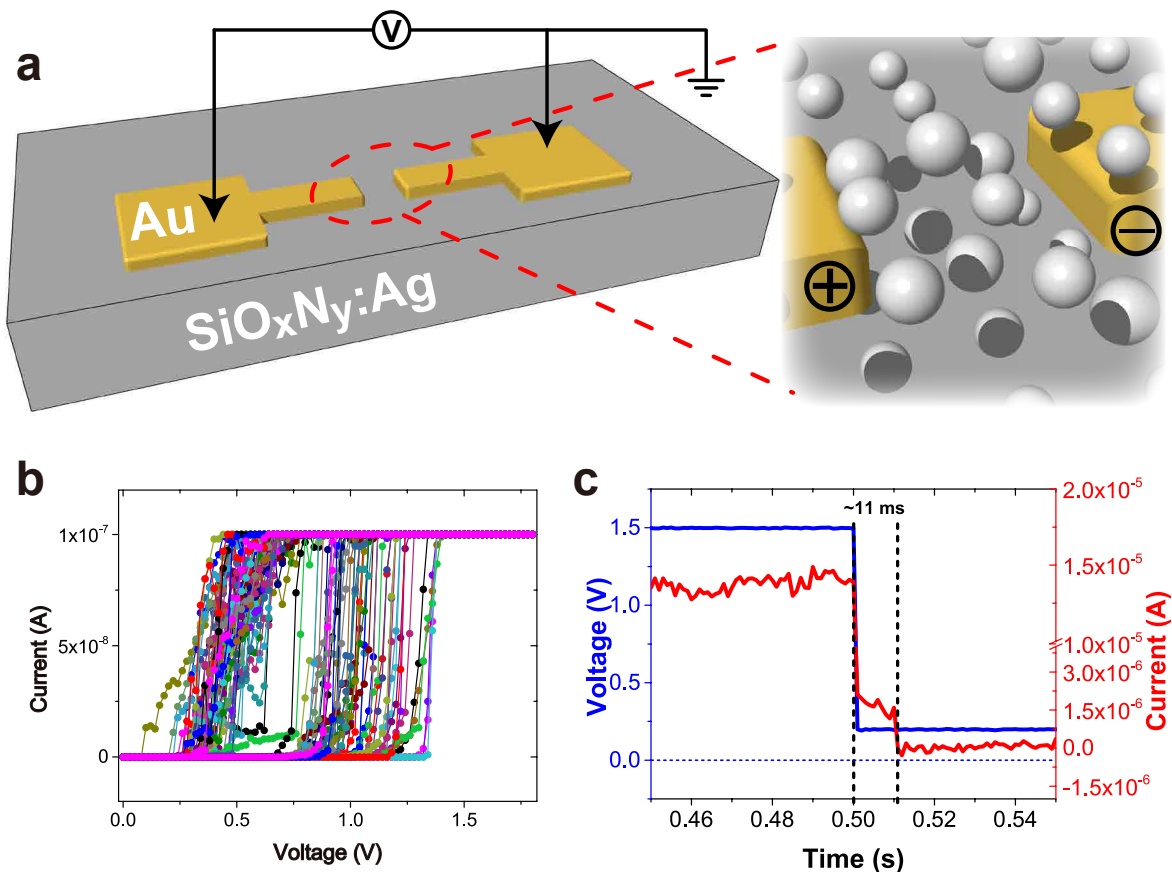
Supplementary Figure S2 HRTEM of Ag nanoclusters in $\text{SiO}_x\text{N}_y:\text{Ag}$ film. The lattice fringes are indexed to Ag (111) plane in (a) (b) and (c). The (d) indicates face-centered cubic structure of the embedded Ag nanoparticle.



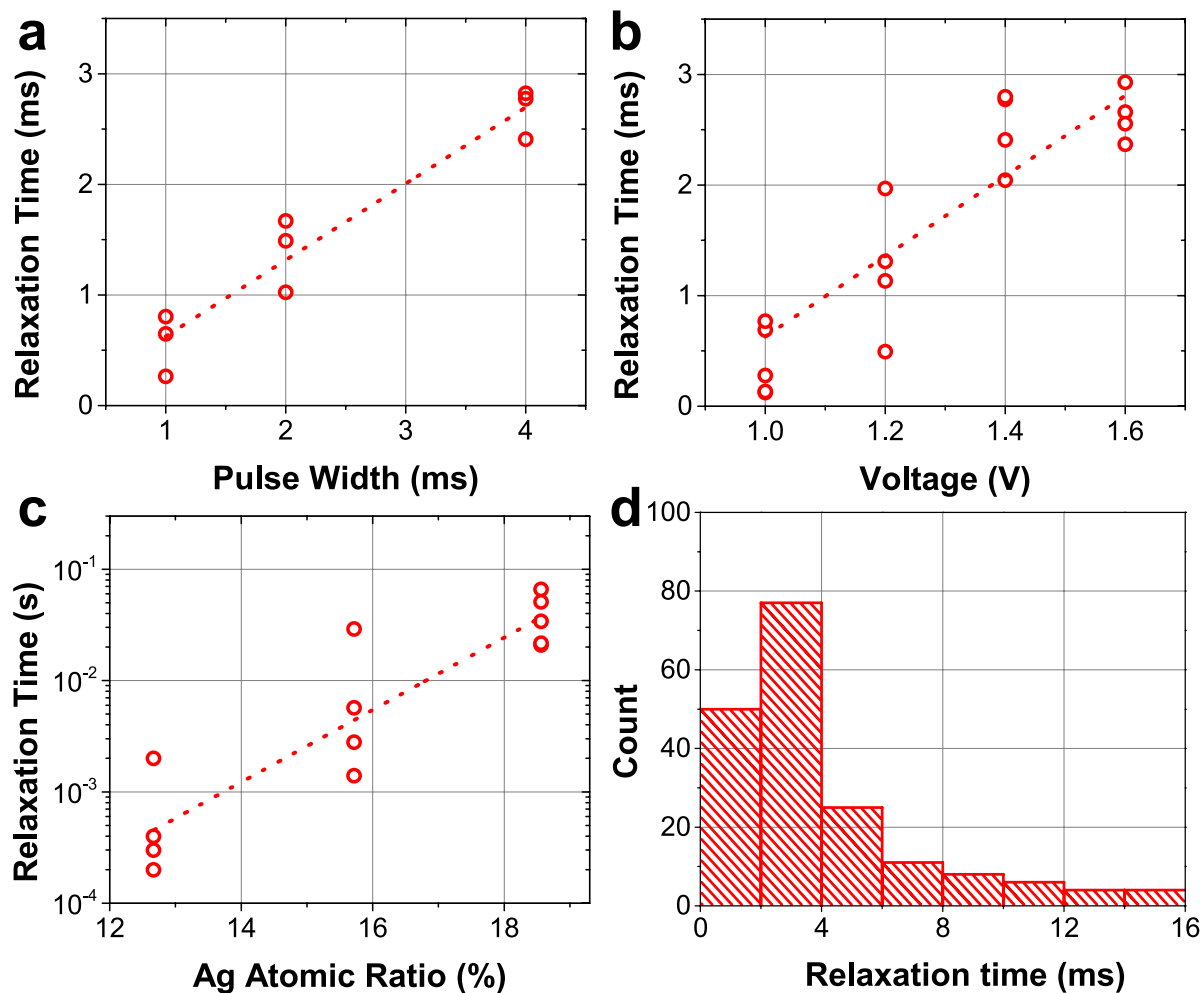
Supplementary Figure S3 The bipolar threshold switching current-voltage characteristics of a crossbar Pt/SiO_xN_y:Ag/Pt diffusive memristor device.



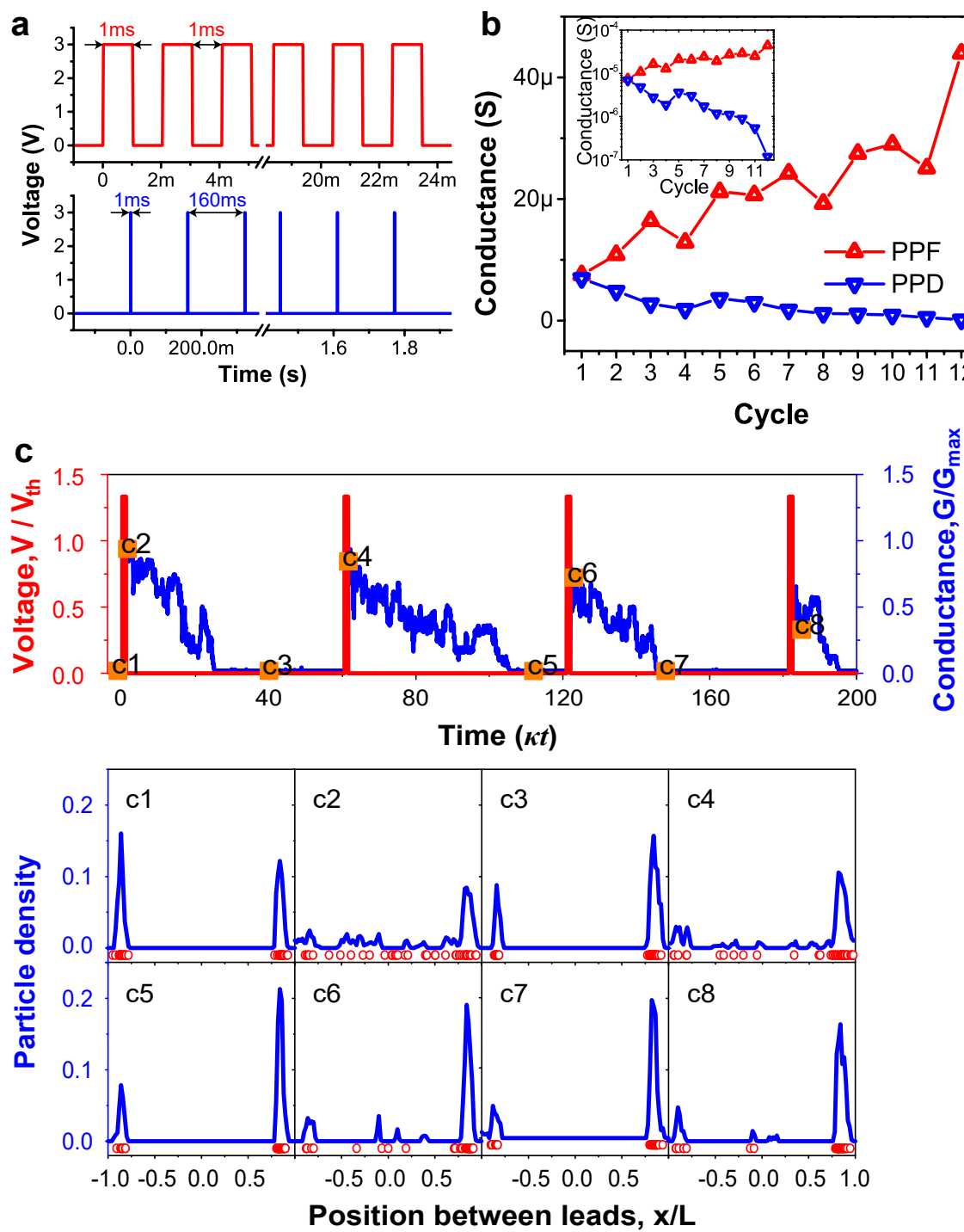
Supplementary Figure S4 Nanoscale crossbar Pt/SiO_xNy:Ag/Pt diffusive memristor and its electrical performance. (a-b) Scanning electron micrographs of the nanoscale crossbar junctions. (c) The current-voltage characteristics of the device.



Supplementary Figure S5 Electrical characteristics of $\text{Au}/\text{SiO}_x\text{N}_y:\text{Ag}/\text{Au}$ lateral diffusive memristor (a) Schematic of the planar structure with two gold electrodes embedded in the dielectrics employed for *in situ* HRTEM. The inset shows the clustered Ag within the gap region serving as bipolar electrodes under biasing. (b) The DC current-voltage characteristics showing repeatable threshold switching in ambient conditions. (c) A typical plot of the time-dependent relaxation of device current when a 2 V excitation pulse followed by a 0.2 V reading pulse is applied in ambient condition.

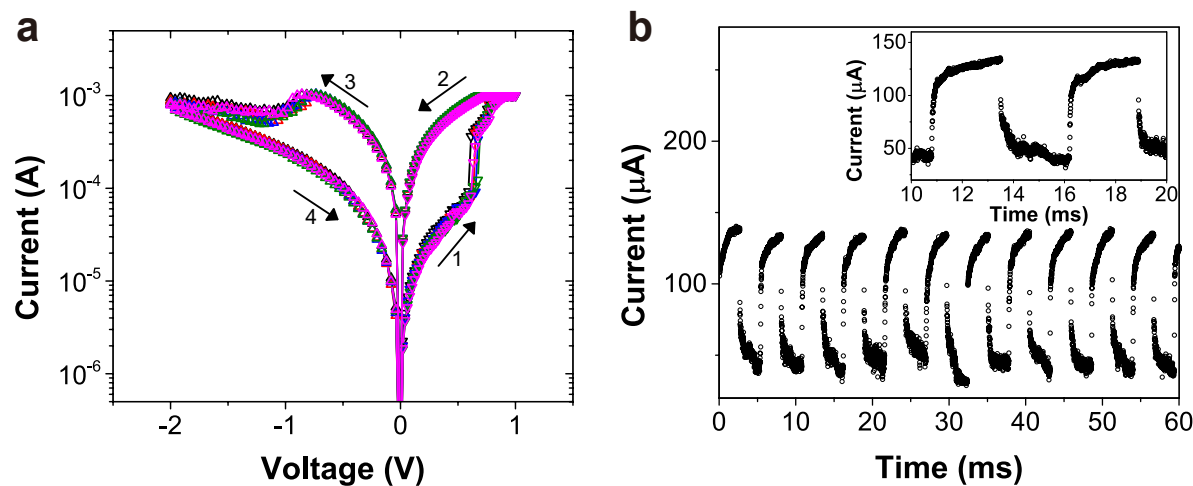


Supplementary Figure S6 The general trend in the variation of relaxation time as a function of pulse width, applied pulse voltage, and the atomic concentration of Ag. (a) The relaxation time increases as a function of pulse width. The pulse voltage used here was 1.4 V. (b) The relaxation time increases with pulse voltage. Here the pulse width was 4 ms. (c) The relaxation time increases with the rising atomic ratio of Ag in the co-sputtered SiO_xN_y:Ag (see the methods section). The pulse was 1 V with a 4 ms width. (d) Histogram plot of the relaxation time of the diffusive memristor extracted from 200 measurements. The applied pulse width and voltage in each independent measurement were 4 ms and 1.5 V, respectively.

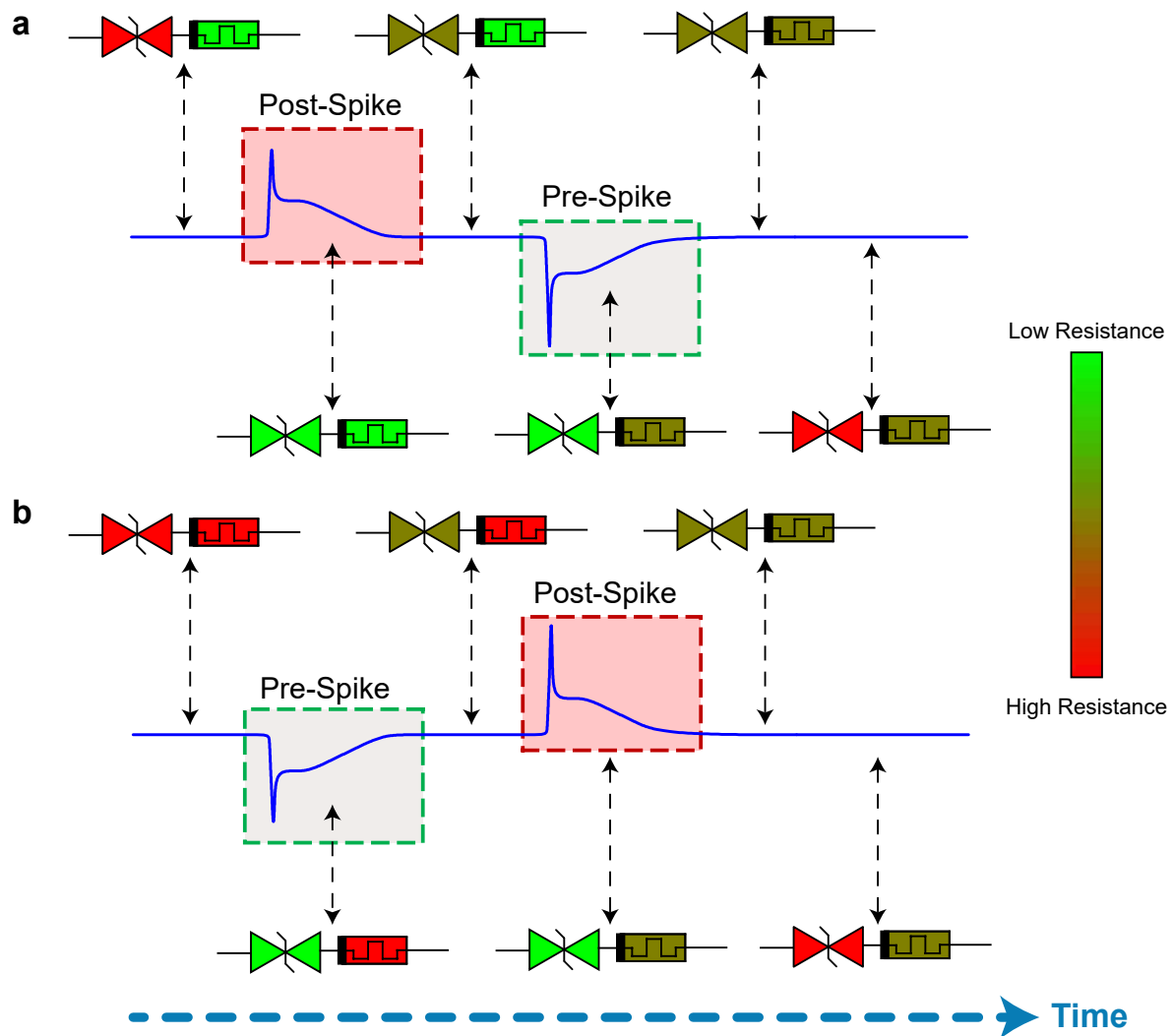


Supplementary Figure S7 Short-term synaptic plasticity with the diffusive $\text{SiO}_x\text{Ny:Ag}$ memristor (a) Illustration of the voltage pulse train for both PPF and PPD demonstrations. The interval between adjacent 3 V pulses is 1 ms (160 ms) for the PPF (PPD) case. (b) The evolution of conductance as a function of the pulse cycles applied to the device. The device is in its steady state before stimulation in both cases. The conductance increases in the PPF case and decreases in the PPD case. Plotted in the inset is the device conductance in log scale (c) The conductance response (blue curve) of the device due to the higher amplitude and sparse train of pulses (red

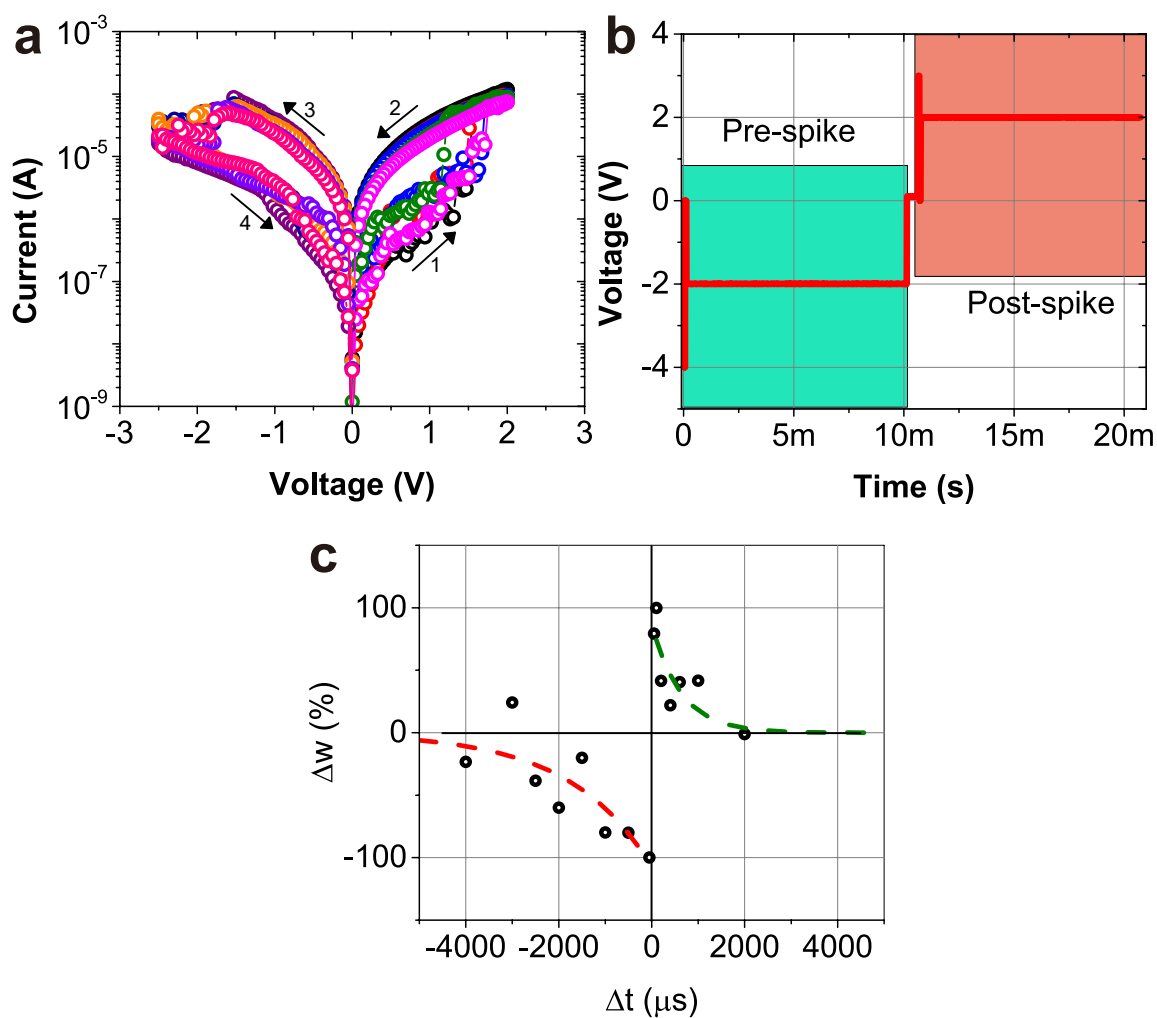
curve) demonstrating PPD; facilitation does not occur since the first pulse excites enough particles to form a bridge between the device terminals and the system completely relaxes to its low conducting state between sequential pulses. Therefore, no excited particle exists between terminals when the next pulse arrives (see, e.g., c1-c3 or c3-c5). The suppression of conductance by the number of pulses still happens due to depletion of left main cluster (compare left and right peaks in the distributions c1, c3, c5, c7), therefore, less and less particles are excited to build a conducting bridge between the terminals (compare c2, c4, c6, c8). Details of simulations and parameters used are described in the methods section and in the caption of Fig. 4 (main text). Note, the depletion saturation can occur due to, e.g., (i) inter-particle repulsion discussed in Ref. 1, and (ii) a diffusion flux against density gradient which is fully taken into account in the model described here.



Supplementary Figure S8 Analog switching behaviour of the Pt/TaO_x/Ta/Pt drift memristors used for the spike-rate-dependent plasticity demonstration of the Figure 6b and 6d
(a) Typical DC current-voltage characteristics of the device. The forming voltage was ~ 6 V
(b) Pulse based switching response. Plot shows the read current following each pulse in subsequent programming operations on the device. The programming pulse width was 300 ns, the set voltage was 0.7 V, reset voltage was -1 V, and the read voltage was 0.1 V.



Supplementary Figure S9 Illustration of states evolution in a STDP protocol (a) An example of the evolution of states of both the diffusive and drift memristors during the depression process. The post-spike turns the diffusive memristor ON. The conductance of the diffusive memristor decays to a certain level after the post-spike. The high voltage peak of the pre-spike decreases the conductance of the drift memristor. The conductance of the diffusive memristor decays and it turns OFF after the pre-spike. (b) An example of the evolution of states in the potentiation process. The pre-spike turns the diffusive memristor ON. The conductance of the diffusive memristor decays to a certain level after the pre-spike. The high peak of the post-spike increases the conductance of the drift memristor. The diffusive memristor conductance decays and it turns OFF after the post-spike.



Supplementary Figure S10 STDP with a Pt/HfO_x/TiN drift memristor (a) Typical I-V Pt/HfO_x/TiN drift memristors used for STDP demonstration with a forming voltage of ~ 4 V. (b) An example of the actual pre- and post-synaptic voltage spikes applied across the device for STDP demonstration. The pre-spike consisted of a $50\ \mu$ s/4 V pulse for programming the drift memristor followed by a $10\text{ ms}/2$ V pulse for programming the diffusive memristor. The post-spike had a $50\ \mu$ s/3 V pulse followed by a $10\text{ ms}/2$ V pulse. We performed five measurements at each time difference Δt and an average was calculated to plot the STDP characteristics. In order to normalize the STDP plot to 100%, the weight change was taken to be equal to the ratio of the change in conductance due to programming and the high conductance value. (c) Plot of the conductance (weight) change of the drift memristor with change in Δt showing the spike-timing-dependent plasticity of the electronic synapse. This response is characteristic of the timing-dependent response of biological synapses.

Reference

- 1 Yi, W. *et al.* Quantized conductance coincides with state instability and excess noise in tantalum oxide memristors. *Nat. Commun.* **7**, 11142, (2016).